



Hybrid manufacturing of steel construction parts via arc welding of LPBF-produced and hot-rolled stainless steels

Martina Chierici¹ · Ali Gökhan Demir² · Alper Kanyilmaz¹ · Filippo Berto³ · Carlo Andrea Castiglioni¹ · Barbara Previtali²

Received: 3 October 2022 / Accepted: 6 June 2023
© The Author(s) 2023

Abstract

The demand for free-form steel structures having improved performances, reducing labour and resource usage is increasing in the construction sector. Structural nodes are some of the most critical regions for steel structures characterised often by large dimensions. These nodes can exploit the geometrical freedom of metal additive manufacturing (MAM) processes. Laser powder bed fusion (LPBF) is arguably the most developed MAM process, which has limitations regarding the size of the parts to be produced. A way to overcome the size limits of LPBF for producing structural nodes while still exploiting its geometrical capacity is producing hybrid components by welding them to traditionally manufactured beams. Such hybrid joints would constitute a complex system from a mechanical design perspective requiring a systematic analysis in order to be certified for structural use. Accordingly, this work studies the mechanical behaviour of hybrid steel components generated by welding LPBF plates and quarto plates made of AISI 316L stainless steel. The work was guided by a case study based on a large steel node, which helped defining the requirements to fill the gap of the international standards. The mechanical characterisation of LPBF-produced plates and quarto plates, as well as the welded hybrid components revealed a maximum of 10% difference between the properties of the differently manufactured plates. Through the digital image correlation (DIC) analyses, the anisotropic deformation behaviour along the LPBF, weld seam, and quarto plate regions have been identified, and the properties after welding did not show relevant modifications. The tests allowed to define that the failure behaviour is mainly governed by interlayer bounds, and a 0.9 safety reduction parameter for considering the reduction of ductility induced by arc welding to LPBF. Finally, design and production suggestions have been provided for a correct evaluation of gross and effective sections of the designed nodes.

Keywords Steel structures · Hybrid complex joints · Laser powder bed fusion · Additive manufacturing · Hybrid manufacturing

1 Introduction

The design of steel structures is becoming more demanding for lightness, optimisation to the performances and efficiency in terms of resource use. It is well known that

structural nodes and their assembly are the most critical features of steel structures, having a low level of optimisation and several design restrictions due to their producibility. Traditional manufacturing for steel structures generally includes forging, rolling and extrusion [1], characterised by high production rates and well known processes for regular-shaped components. However, when dealing with complex geometries or high customisation, the favourability of traditional techniques reduces, with an increase of design costs and labour content.

A current obstacle that nowadays designers and manufacturers are facing is the design and production of complex structural nodes for free-form or high performance structures. These nodes are often composed of several separately manufactured parts, meeting with several different angles.

✉ Ali Gökhan Demir
aligokhan.demir@polimi.it

¹ Department of Architecture, Built Environment and Construction Engineering, Politecnico di Milano, Milan, Italy

² Department of Mechanical Engineering, Politecnico di Milano, Milan, Italy

³ Department of Chemical Engineering Materials Environment, Sapienza, Università di Roma, Rome, Italy

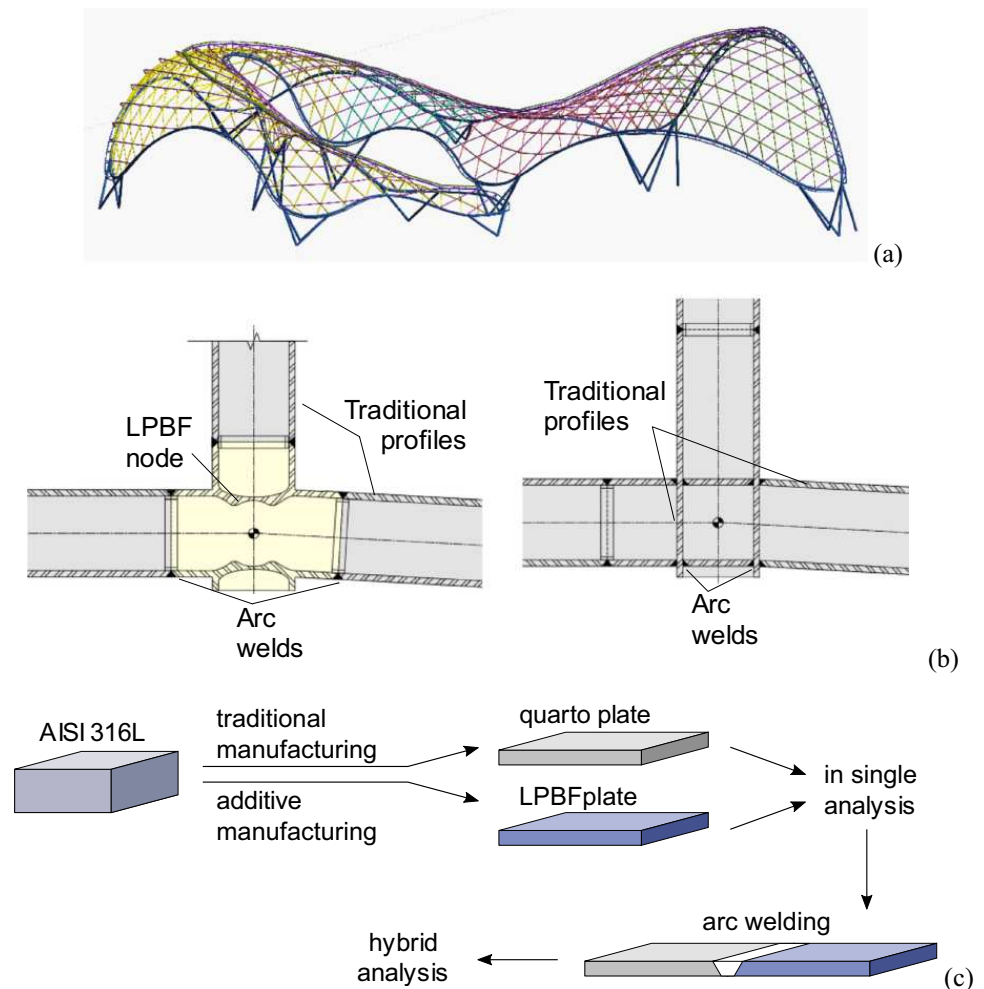
The assembling process requires shaping the beams edges to fit nodes' geometry, and high quantity of bolted connections or metres of welding. Then, when the beams are made of hollow sections, the need for internal stiffeners adds further cutting and welding operations, as well as geometrical discontinuities and stress concentration regions. In addition, unique design for several nodes is often required, also in the same structure, making the design cost and the labour content drastically increase.

On the basis of the rising steel structure requirements for resource efficiency, simplified assembly and optimised design can find a beneficial tool in metal additive manufacturing (MAM) [2–4] for the production of structural nodes [5–12]. By employing optimised additively manufactured nodes to join traditionally manufactured large regular-shaped profiles, MAM can find a favourable and sustainable use in the construction sector (Fig. 1a) [8, 13]. Indeed, this solution exploits the advantages and meets the limits of both traditional and additive manufacturing. Traditional steel manufacturing ensures a low costs, high productivity, and efficiency in the production of structure's columns and

beams. On the other hand, using additive manufacturing to produce the complex nodes, it is possible a low-cost shape and assembling optimisation [10] reducing in shop work, on-site labour and scraps [14]. In addition, nodes having medium dimensions agree with most of MAM processes including laser metal deposition (LMD) and laser powder bed fusion (LPBF). A previous work from the authors [15] demonstrated that additively manufactured structural nodes can save up to 90% of the scraps from their traditional manufacturing, 20% of their weight, and almost 45% of the CO₂ emission from transportation. However, the required energy for the additive manufacturing was estimated higher than the needed for traditionally manufacture the nodes. From the structural point of view, with MAM-produced nodes, the stress concentration is reduced, and any need for welding is limited to the on-site assembling (Fig. 1b). The reduction in number of assembling operation can also simplify the capacity design of the whole structure, improving its safety and reducing the need for oversizing [15].

Despite the advantages that MAM can provide to the steel construction industry, the design and verification of

Fig. 1 Scheme of the case study steel structure which requires complex node geometry (a). AM produced and traditional node with the required welding for the node production (b). Processes involved in the production of the samples (c)



components for steel structures are strictly related to the design codes. The international standards define rules for the traditional manufacturing techniques and the typical nodes' shapes. Concerning non-certified production processes for structural steel, such as MAM, several regulations are not applicable, and the products properties need to be certified to guarantee their compliance with the requirements stated by the standards. In detail, the steel conformity for structural components can be studied according to EN 1090-1 [16], which states the rules for products from hot rolling, cold forming and other technologies. It refers to the strength properties, the weldability and fracture toughness proposed in EN 1090-2 [17], even if this code is specific for the execution of steelwork produced from hot rolling, cold forming and hot finishing. This specification limits the use of EN 1090-2 [17] for MAM products design to those rules referred to by EN 1090-1 [16]. Moving forward to the design of steel structures (Eurocode 3 Part 1-1 [18]), the material properties of nonstandard products need to be tested, and the conformity to the values presented in EC3 1-1 section 5.2 need to be checked. In addition, the supplementary rules for steel structures of Eurocode 3 Part 1-4 [19] can be applied when the material properties are in accordance with the values it sets. Going into the detail of the design of joints (Eurocode 3 Part 1-8 [20]), the standard refers to EN 1090-2 [17] for admitted products. Since EN 1090-2 specifies the requirements for the execution of structural steelworks produced just from hot rolling, cold forming and hot finishing, steel joints can be designed according to the standards just if made by the specified products. However, the use of alternative production processes for structural steel is allowed, but the design and verification need to be subject to a certification body.

On the base of the analysis of the international standards, the first step for designing a structural steel component produced with MAM is the qualification of its properties, and the reliability of possible connections with other parts. A literature review on MAM steel products revealed that their mechanical properties at the lab scale are comparable to traditional steel [22–23], and they demonstrated an anisotropic behaviour. Experimental works also proved the dependency of MAM product properties on process parameters [24], which are designed for the required geometry, lead time and special features. Other relevant factors determining behaviour of the component are the post-process treatments [26–29], whose choice depends on the desired resulting properties, part shape and dimensions. Concerning the techniques to join several parts, one of which produced with MAM, in the literature there are a few works dealing with laser welding of LPBF-manufactured steel plates [31–32], which induced modifications on the involved metals. The use of LPBF to directly manufacture on existing parts have been assessed in the literature as well [33, 34]. Such strategy would require flat surfaces to build the LPBF-produced part

and the part sizes would be limited to the volume of the used machine. The literature on the arc welding of LPBF-produced steels and in particular hybrid joints is very limited. In Pasang et al. [35], arc-welded 2.5-mm-thick steel plates produced by LPBF showed promising results in terms of mechanical properties. However, for the construction industry, a greater understanding of the mechanical properties is required for higher thicknesses (> 8 mm) and hybrid joints. Civil construction being one of the most conservative sectors in terms of design regulations, requires fundamental studies dealing with material properties in this new application field [36]. To authors' knowledge, no previous work has attempted to assess the mechanical properties of welded MAM-traditional steel configurations in the light of the civil construction requirements.

For proving the suitability of using MAM for the production of a structural node for traditional steel beams, some challenges are still present. As stated by the international standards, the materials and joints properties need to be specified for non-standards products. The literature did not revealed a sufficient stability for MAM processes and materials properties for thick components. Thus, an experimental study has been set for a comprehensive quantification of the mechanical and physical properties of MAM thick steel parts produced for high productivity. Concerning the reliability of joining the MAM node to traditionally manufactured beams, there is a huge lack of knowledge about the quantification of the thermal effect of welding on thick steel parts. Thus, an experimental investigation is needed to identify the weak regions and to quantify the MAM products properties variation induced by welding.

On the basis of the current knowledge gap that prevents a favourable use of MAM in the construction sector, the authors propose the present work. Laser powder bed fusion (LPBF) is the considered MAM process, owing to its industrial maturity. Indeed, it has a great degree of geometrical freedom compared to laser metal deposition and other directed energy deposition processes. AISI 316L with its common use in special steel structures, known LPBF processability [37] and good weldability [16] was chosen as the material. To analyse material properties, thick plates have been considered, setting the thickness to 10 mm, in order to meet the dimension-dependant parameter of LPBF process, as well as the properties dependency on the heat effect induced by fusing several subsequent layers. The LPBF 10-mm-thick plates were produced with different orientations to extensively characterise the material concerning porosity, microhardness, microstructures, tensile strength and anisotropy. The needed assembly process for the designed MAM node should be applicable on-site, which better fits the process properties of manual arc welding, as commonly employed in the construction industry. The reliability of arc welding for assembling LPBF AISI

316L to traditionally manufactured steel beams is investigated by arc welding LPBF 10-mm-thick plates (produced with different orientations) to the traditional counterparts. The experimental analysis on the welded joint concerned the same properties investigated for the base material, in order to quantify the integrity of the welded joint, and the effects of welding thermal cycles on the materials properties. Digital image correlation (DIC) was applied during tensile tests determining the strain development in the welded samples, and revealing the heterogenous strain behaviour among the welded specimens. The results were then related to the design process for structural nodes, and the needed verifications for a safe employment of LPBF in the construction sector were outlined. A visual outlook of the production processes of the sample is presented in Fig. 1c.

2 Materials and methods

This study began with the material choice, the production of the samples, and the identification of the analyses to perform. The study pointed at investigating the changes induced on LPBF-produced AISI 316L by the thermal cycles from arc welding. Indeed, the large thickness of the plates requires several welding layers, and the effect of a concentrated heat source on LPBF steel is still unknown. The metals in both single and welded hybrid configurations were studied also to relate the welded joints properties to the base metals, and thus provide possible correcting parameters to quantify the mechanical properties of welded joints starting from the base metals ones.

2.1 Feedstock material

The test material was chosen to meet the typical mechanical properties required to metals for structural applications [16] and the processability for LPBF [37]. AISI 316L was selected for both additive and traditional manufacturing (respectively LPBF and quarto plates) with the same nominal chemical composition. Table 1 reports the chemical composition of the quarto plates and the powder feedstock used in the experiments. The steel for LPBF process was gas atomised and sieved to produce powder having a size distribution between 18 and 47 μm (Höganäs, Goslar, Germany). For the production of quarto plates, AISI 316L ingots were hot rolled to the thickness.

Table 1 Chemical composition of the quarto plate steel and of the powder used for LPBF

Mass %	C	Si	Mn	P	S	Cr	Ni	Mo	N	O	Iron
Quarto plate	0.017	0.50	1.35	0.027	0.002	17.0	10.1	2.04	0.04		Balance
Powder	0.00	0.20	1.51	<0.010	0.004	17.7	11.9	2.3	0.01	0.04	Balance

2.2 Quarto plate production

Quarto plates are hot-rolled products, and we considered them for sake of simplicity as representative products for traditional manufacturing. Their analysis has been used to compare the physical and mechanical properties of the LPBF products. They have been then employed as the counterpart of LPBF plates for the investigation of the hybrid joint, representing the LPBF node welded to traditionally manufactured beams. Quarto plates are obtained by rolling ingots produced by converting iron, or by means of fusion of metal scraps and iron ore. The rolling process requires the use of heated ingots up to work with softened material. The material pass through a series of counter-rotating rollers which shaped the plate to the designed thickness [1]. AISI 316L quarto plates were provided by, Finland.

2.3 Laser powder bed fusion of the specimens

An industrial LPBF system was employed for the production of the plates (Renishaw AM250, Stone, UK). The employed LPBF system is equipped with an active fibre laser operating in pulsed wave (PW) emission by power modulation [38]. The laser scans continuous scan tracks, while the laser is modulated with the given exposure time (t_{on}) emitting pulses with a fixed point distance (d_p) [39]. Meander scan strategy was used, while the scan direction was varied by 67° between each layer. The system operated under Ar atmosphere, maintaining the oxygen level below 1000 ppm. The process parameters were set to produce parts with sufficient density and high productivity. Laser power (P) was set at 200 W, with an exposure time of 80 μs , while point (d_p) and hatch (d_h) distances were set at 60 μm and 110 μm respectively. Layer thickness (z) was 50 μm . The plates were designed to have 10 mm thickness, 70 mm length and 90 mm width for the consecutive gas tungsten arc welding (GTAW) process. Plates were produced with different orientations to test the influence of material anisotropy with respect to the build direction as shown in Fig. 2a. The produced specimens are shown in Fig. 2b. All specimens were tested after a sand-blasting operation to remove the sintered particles. No heat treatment was applied to the tested specimens.

2.4 GTAW of hybrid specimens

GTAW was used to weld LPBF specimens to quarto plates since it is a widely used welding process in the

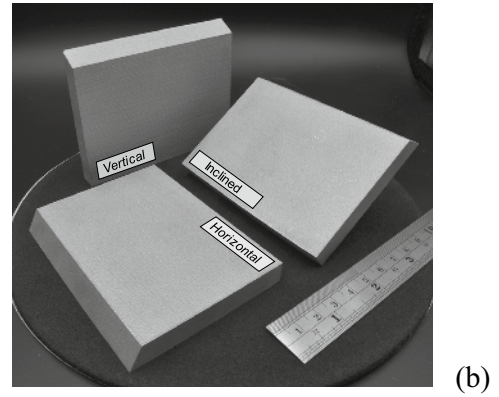
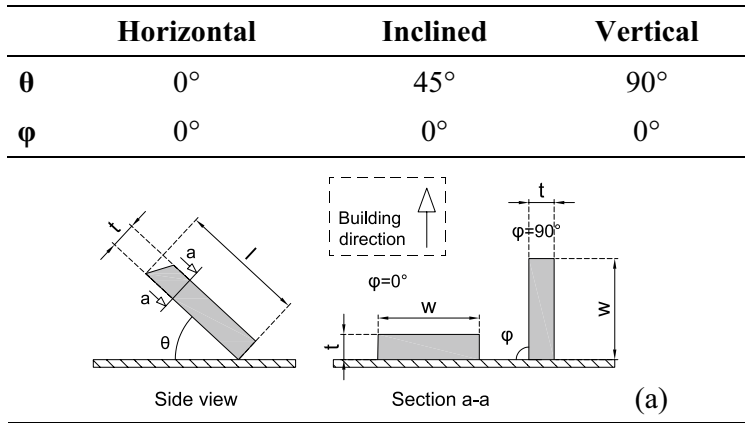


Fig. 2 Build orientation angles θ and φ for LPBF, and dimensions nomenclature (a); produced specimens having $t=10$ mm, $l=70$ mm, $w=90$ mm (b)

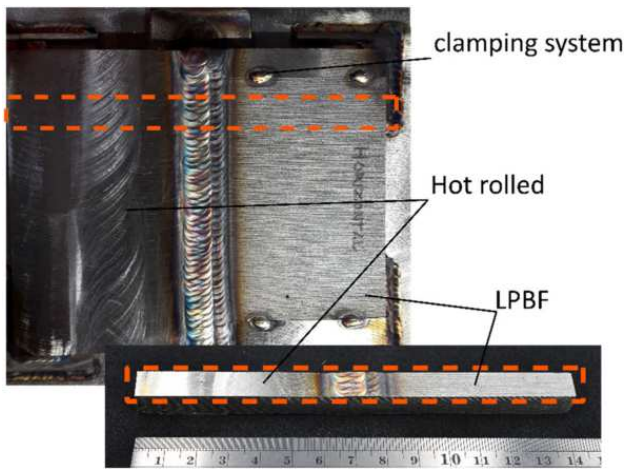


Fig. 3 Welding setup and extracted sample. Marker in cm

construction sector [17, 40]. An expert weld engineer configured a butt joint as designed for the optimised structural node (Fig. 1b). A clamping system to reduce the heat-induced deformations was employed, maintaining the sample straight during welding. The expert applied manually the welds with 7 consecutive passes using AISI 316L as the filler wire (Fig. 3). No surface finishing was applied after welding, and the excess of metal on the weld seam was not grinded to test the most severe condition. The quality of the welds was confirmed through dye penetrant tests and radiographic tests according to the respective codes [41, 42].

2.5 Characterisation

LPBF is not yet present in the current standards as a manufacturing process for structural steel. Therefore, its suitability should be proved by proper qualification and certification pathways (as proposed by certification bodies [9]). Proposing products having properties which suit the structural steel requirements according to the international standards EN 1090-2 [17] would simplify the approval process. With this aim, the surface quality of the as-built products was evaluated to identify possible finishing processes to obtain the standard roughness for structural steels, and to quantify the gross section of the LPBF components to guarantee sufficient thickness for the resisting section after sanding. It is well known that the metallographic properties are strictly dependant on the production process, and that they determine the mechanical properties. Thus, porosity, microhardness, microstructure and tensile properties provided the information to investigate the quality of thick LPBF products with high productivity parameters. In addition, the properties were used to study the effect that the concentrated thermal cycle of the seven layers of welding had on the LPBF steel. Specifically, the tensile tests were designed to study the strength of the welded samples, and to investigate the fracture location and the local properties of the welded metals. The comparison to the base metals properties aimed to quantify possible performance modifications due to the seven-layer welding. In addition, the gathered properties represent the needed data to build reliable numerical models of the structural nodes to assess their integrity with reduced prototype testing.

2.5.1 Surface roughness

A tactile surface roughness measurement system (Mahr Perthometer, Göttingen, Germany) was used to measure

the roughness parameters for both the LPBF and quarto plates. For LPBF plates measurements were carried out in three locations for each plate: top, bottom and groove face (edge) (Fig. 4), considering as measure direction the build direction.

2.5.2 Metallography

LPBF-produced and quarto plate specimens were cut and mounted in resin and prepared for metallographic analysis by conventional grinding and polishing methods. Optical microscopy of the cross-sections was taken to measure the level of porosity. Vickers microhardness profile along the longitudinal direction of the samples was taken according to ISO 6507 [43] to outline variation of the mechanical properties in LPBF, quarto plate, welded zones. Microhardness profiles were taken at three different heights along the plate thickness, applying a 10 N load, with a dwell time of 5 s. Material microstructure was revealed by chemical etching, with a solution composed of one HNO₃ part, one HCl part and one part of water. The samples were immersed for 45 s in the solution before washing and drying. Optical microscopy and scanning electron microscopy (SEM) images were taken.

2.5.3 Mechanical testing

Tensile tests of the LPBF parts and quarto plates were made to assess the mechanical properties prior to the welding operation. For the hybrid specimens, the welded plates were cut obtaining six tensile testing bars for each orientation having length 143 mm, thickness 10 mm and width 10 mm as shown in Fig. 5c. An extensometer at the longitudinal direction of each sample, and a strain gauge along the transversal direction (Fig. 5b) provided the elongation values to study both the elastic and the post-elastic properties of the materials. To compute the elastic constants of the transversal isotropic LPBF AISI 316L, the strain gauges were applied on the surfaces corresponding to the planes 1–2 (H) (isotropic plane) and 1–3 (VH) (assumed equivalent to 2–3). The

last plane is studied along two directions as an off-axis configuration test in order to obtain the data for the computation of its shear modulus [44]: 1–3 (HV), 1–3 inclined at 45° (I) (Fig. 5a). The Poisson ratios were computed as the ratio between the transversal elastic strain and the longitudinal one of the central cross section of the samples: $\nu = \frac{\epsilon_t}{\epsilon_l}$. Since tensile tests exhibit an unstable initial phase, the strain values for the computation were selected when the stress–strain curve reaches a stable trend, it means after 0.012% strain and 25 MPa.

Tensile tests were carried out under displacement control with a universal testing machine (MTS Alliance RT/100, Eden Prairie, MN, USA) fitted with a digital image correlation (DIC) system (Aramis 3D Camera, Braunschweig, Germany). A speckle pattern was applied to the specimens prior to testing. DIC offers point-by-point strain computation on a pre-defined region of the sample. The acquired images were processed applying “virtual extensometers” to quantify the strains in LPBF and quarto plate sides of the hybrid specimens. After the tensile tests SEM images were taken in the fracture zone was for a better understanding of the failure mechanism.

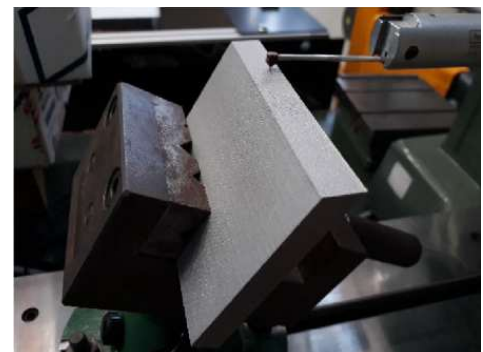
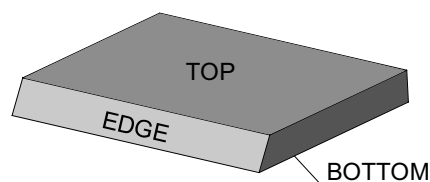
3 Results

A first visual inspection of the LPBF and quarto plate samples did not reveal macroscopic imperfections, and the welding expert performed state-of-the-art welds since no defects were detected. The more specific analyses performed on the samples are presented in the following sections.

3.1 Characterisation of LPBF-produced specimens and quarto plates

The base metals were characterised to provide information about the products quality obtained through high productivity parameters, and the reference values to quantify the welding thermal effect on the LPBF steel.

Fig. 4 Surface roughness measurements reference system, and picture from the measurement



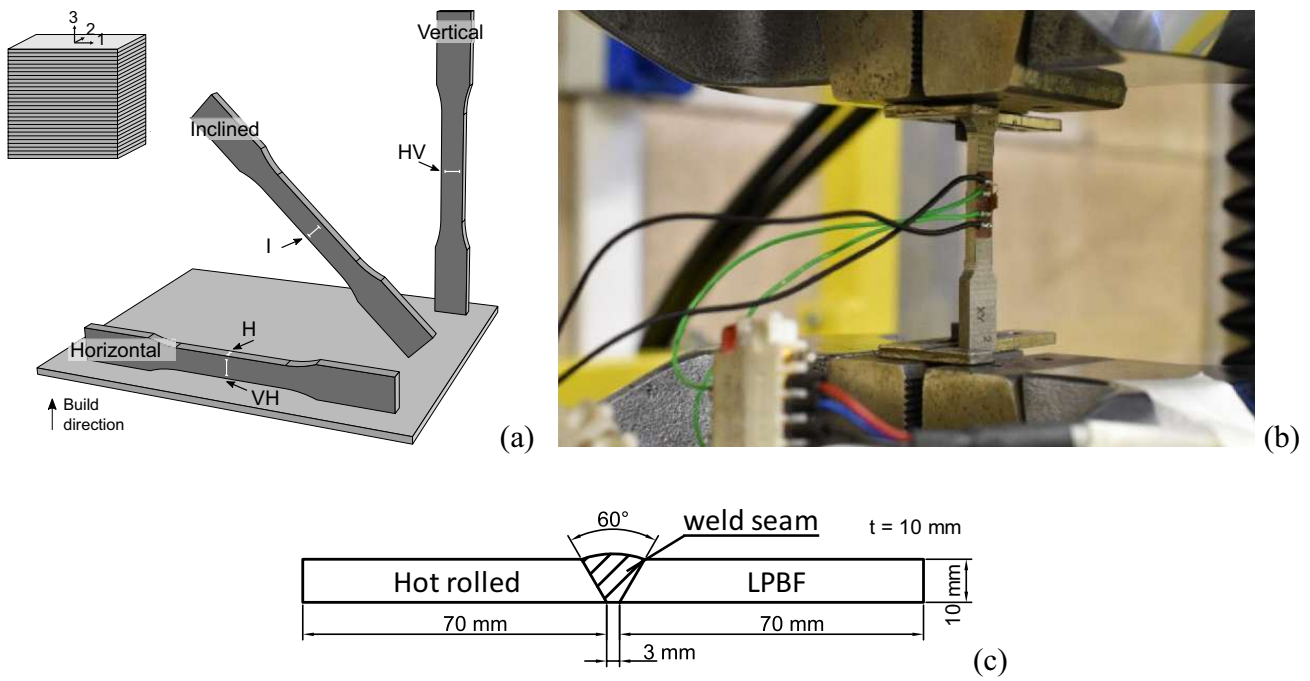


Fig. 5 Strain gauge setting on the three types of base metals sample (a); tensile test setting for base metals with transversal strain gauges (b) geometry and dimensions (mm) of the welded tensile specimens (c)

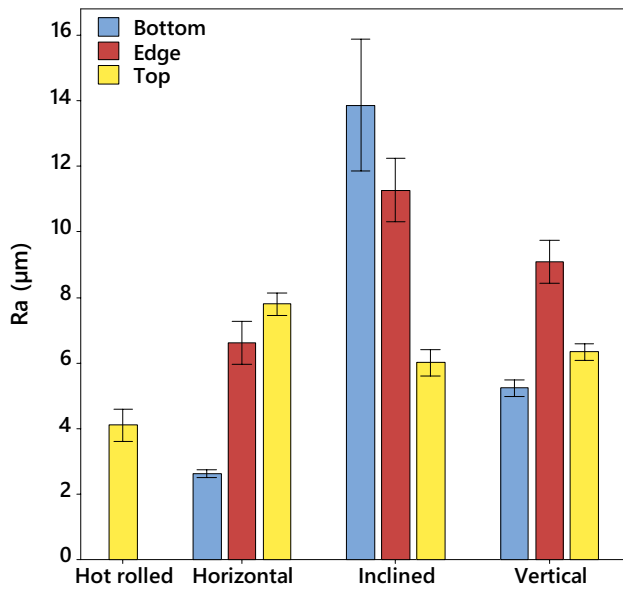


Fig. 6 Measured parameters Ra with standard error for the quarto plate and LPBF base metals (AISI 316L)

3.1.1 Surface quality

Figure 6 shows the average surface roughness of the specimens. The experimental results on the quarto plate revealed smooth surfaces fitting the requirements for structural steel (3.5–7.5 μm) [45], and resulted comparable to the values

from the BOTTOM horizontal (Figs. 2, 4) values of the LPBF sample. Conversely, the BOTTOM inclined set showed the highest Ra. The measured region is characterised typically by a higher roughness as it is sustained by the powder bed during the LPBF process, which results in limited heat dissipation accompanied by a rougher topography. Similarly, observations can be made for to the EDGE inclined and the EDGE vertical regions. The results showed that the surface roughness is anisotropic in the built parts, which may induce different fatigue behaviour in the part as well as possible issues with fitted or bolted assemblies. These results are essential to qualify the best surface finishing process and the quantity of material to remove to reach the standard roughness for structural steel.

3.1.2 Porosity

The average density for the three considered build directions of the LPBF parts did not present great differences: horizontal 99.52%; inclined 99.70%; vertical 99.85%, where non circular pores were observed locally (Fig. 7a). The image analysis allowed to identify small and spherical pores attributed to gas entrapment, and irregularly shaped pores, which may be associated to lack of fusion or spatter induced porosity (Fig. 7a) [46, 47]. Concerning the AISI 316L quarto plate, the average density was close to 100% (Fig. 7b). Since the pores are discontinuities favouring cracks formation and propagation, the density of the base metals, and the

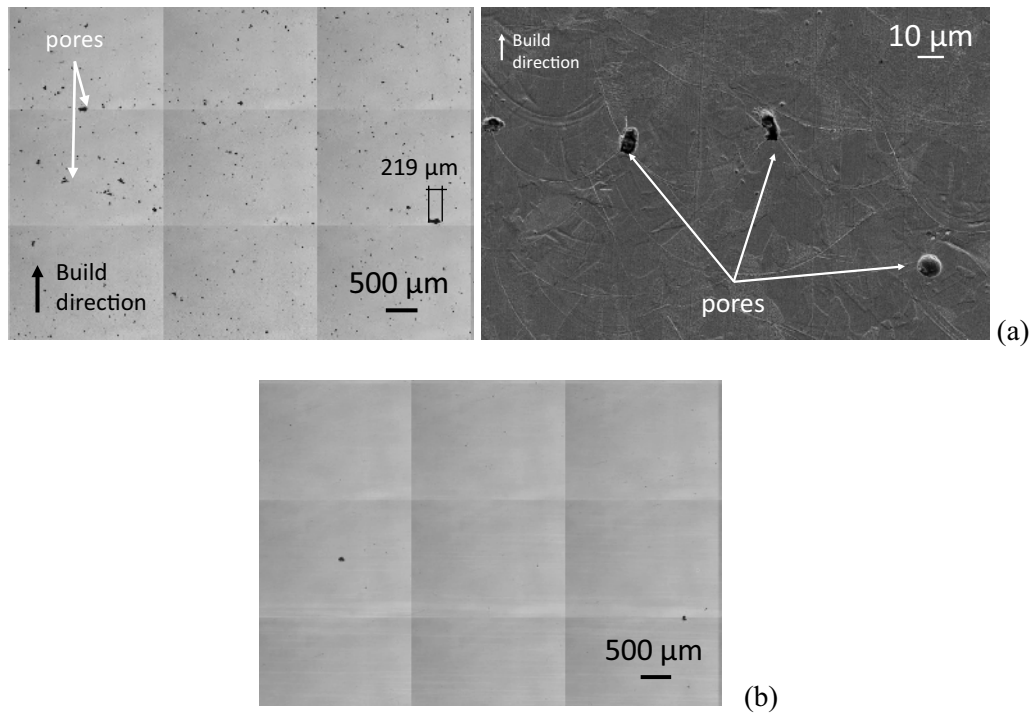


Fig. 7 Analysis for pores in the LPBF-produced horizontal sample (a) and in the quarto plate one (b)

maximum dimensions of the pores suggested the possible influence of the porosity on the mechanical properties of the materials. In addition, the high quantity of pores can be responsible for a low ductility of the materials [48].

3.1.3 Microhardness

Microhardness analyses on the base metals (Fig. 8) revealed that the quarto plate values lied in the recommended typical range for structural steel [49]. On the other hand, the higher microhardness values of LPBF AISI 316L with respect to the quarto plate are associated to the rapid solidification induced during the LPBF process. No sensible difference was observed between the different build directions. This was because the microhardness measurements were carried out along the build direction for each specimen, and in order to better reveal the anisotropic behaviour a macro approach such as the tensile test is required. Overall, the results confirmed the adequateness of both of the materials for further testing, and represented the reference values to quantify the heat-affected zone in the welded samples.

3.1.4 Microstructure

The quarto plates showed both δ -ferrite (Fig. 9a) and annealing twins (Fig. 9b), the grains showed an equiaxed structure, and approximately 30 μm medium dimension. Etching the base LPBF AISI 316L highlighted the melt pools produced

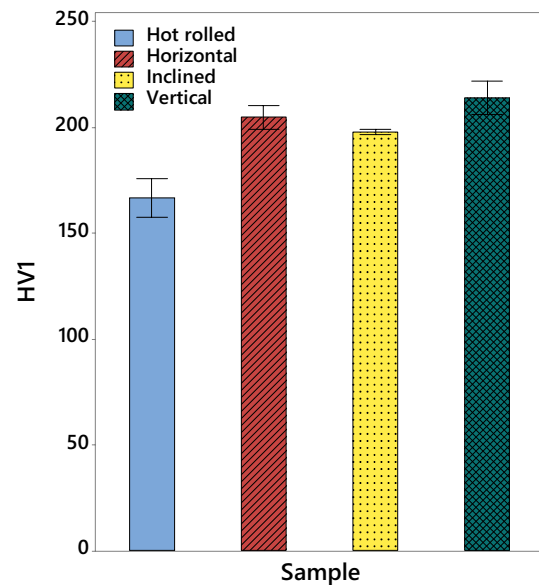


Fig. 8 Microhardness measurement with standard error of the hot-rolled quarto plate and LPBF produced AISI 316L

by the laser scanning, and the specific scan strategy for each build direction. As example, the dashed lines in Fig. 9d depicted the melt pool boundaries of the sample vertical, and the scheme for their measurement. The melt pool width was found to be constant among the three selected build directions (i.e. horizontal, inclined and vertical) approximately at

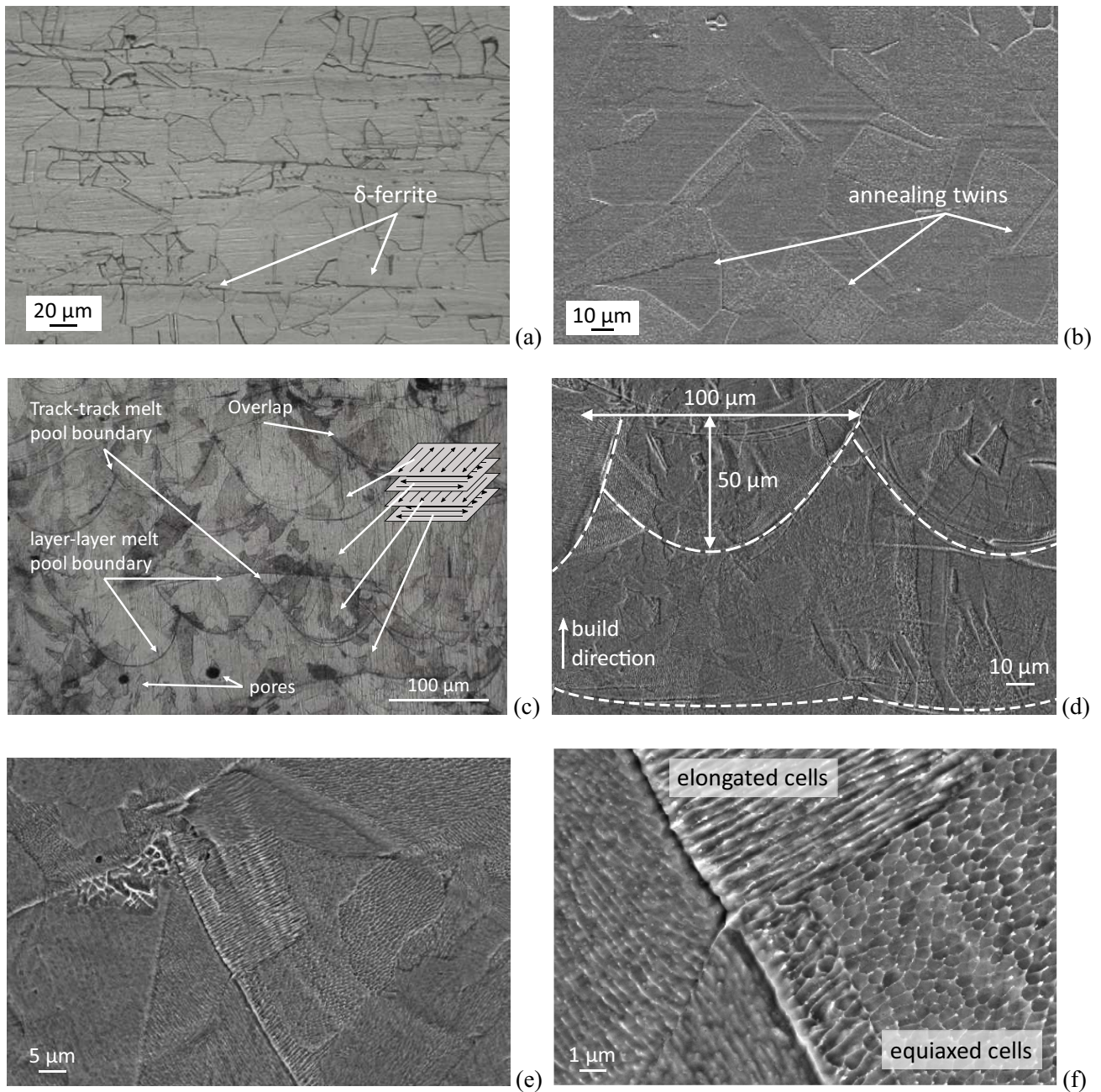


Fig. 9 Microstructure of the quarto plate (a, b) and LPBF vertical specimen (c–f). Equiaxed fine cells in LPBF-produced AISI 316L

100 μm (see Fig. 9d). Partial overlaps of adjacent scan areas (Fig. 9c) were detected during the microstructure observation due to a smaller hatch distance with respect to melt pool width. Elongated grains, oriented along the build direction, spanning over melt pool boundaries was observed in all the LPBF samples. This peculiar morphology is induced by the high cooling rate of LPBF process, and it is the most probable factor which induce the typical LPBF material anisotropy [31]. Further magnification from the SEM revealed

elongated and equiaxed cells in the grains (Fig. 9e–f) within the single melt pools.

3.1.5 Tensile properties

The mechanical properties of the quarto plate and LPBF-produced AISI 316L are shown in Fig. 10, where E is the Young's modulus, $\sigma_{0.2}$ is the 0.2% proof stress, UTS is the ultimate tensile strength, ϵ_u is the elongation at the ultimate tensile strength, ϵ_f is the elongation at failure, and ν is the

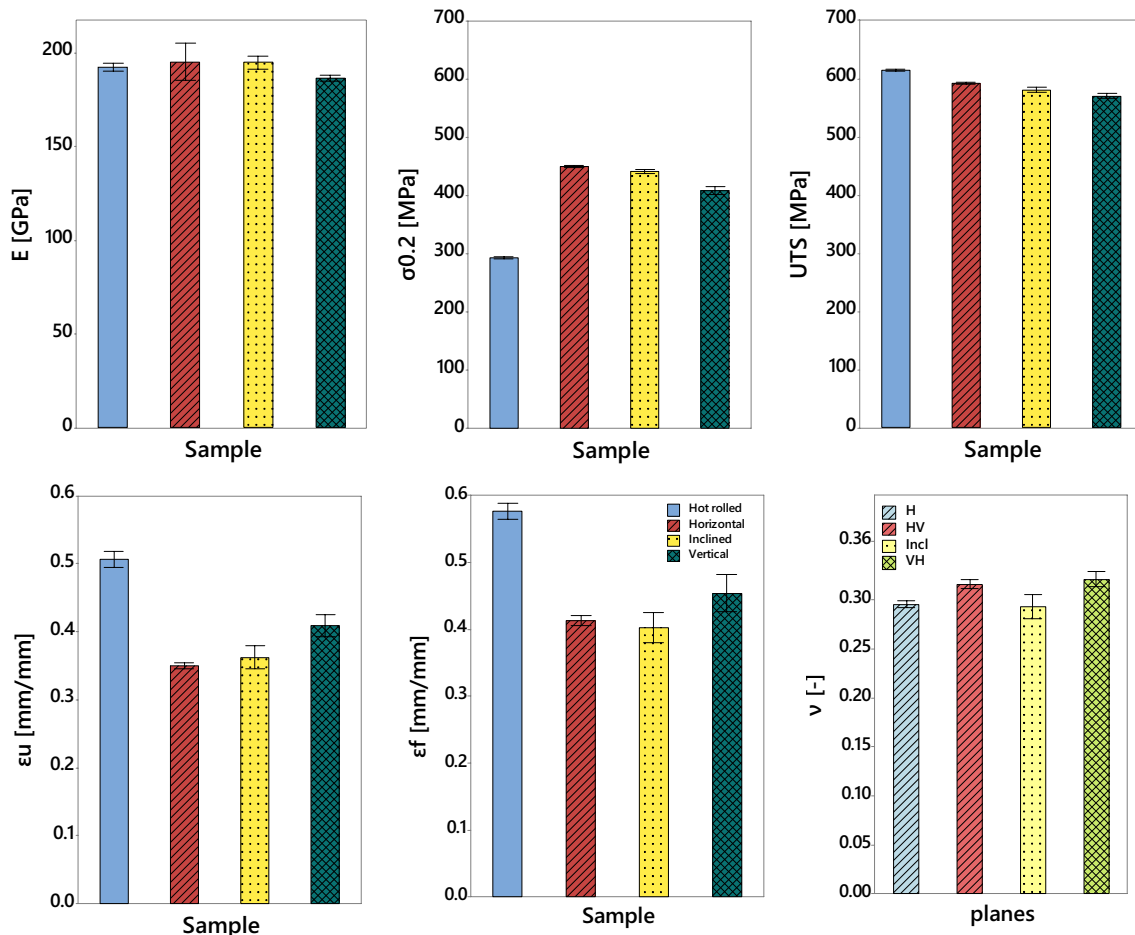


Fig. 10 Experimental values with standard error for the main mechanical properties of the base metals: Young's modulus E , 0.2% proof stress $\sigma_{0.2}$, ultimate tensile strength UTS, strain at ultimate tensile strength ϵ_u , strain at failure ϵ_f , Poisson's ratio ν

Poisson ratio for the LPBF steel according to Fig. 5. The results highlighted a weak anisotropy in all the LPBF samples, and identified the inclined direction as the transition orientation from the horizontal to the vertical directions. All the Poisson ratios are close to 0.3 as typical value of traditional stainless steel, however, the anisotropy reflected also in this property. The LPBF-produced AISI 316L had similar mechanical properties to the quarto plate counterpart in terms of elastic modulus, and ultimate tensile strength. On the other hand, LPBF-produced AISI 316 had a higher yielding point and a lower elongation at break. However, LPBF-produced AISI 316L demonstrated mechanical properties fitting the standard values for stainless steels for structural roles in the construction sector. These results are also essential to quantify the variations induced by the welding thermal cycles on the two involved metals.

The fracture surface observation suggested that the AISI 316L quarto plate was sufficiently dense and ductile to develop a complete ductile fracture (Fig. 11a) with homogeneous ductile dimples and a pronounced necking.

Conversely, the LPBF samples demonstrated a more brittle behaviour, induced by the growth of pores instead of section necking, and the presence of small dimples and brittle fracture surfaces (Fig. 11b). These observations confirmed that the pores increased the brittleness of the LPBF-produced sample.

3.2 Characterisation of the welded hybrid samples

Porosity, microhardness and microstructural analyses have been performed on the hybrid joints to quantify the effects that the seven welding layers had on the base metals. The results allowed to identify the variation from the properties of the base materials, quantify the dimension and the properties of the heat-affected zones. The data provides the needed information to build accurate numerical models able to capture the possible weakening of materials due to welding. Numerical and analytical analyses would prove if the standard design rules [18] offer reliable approaches also for

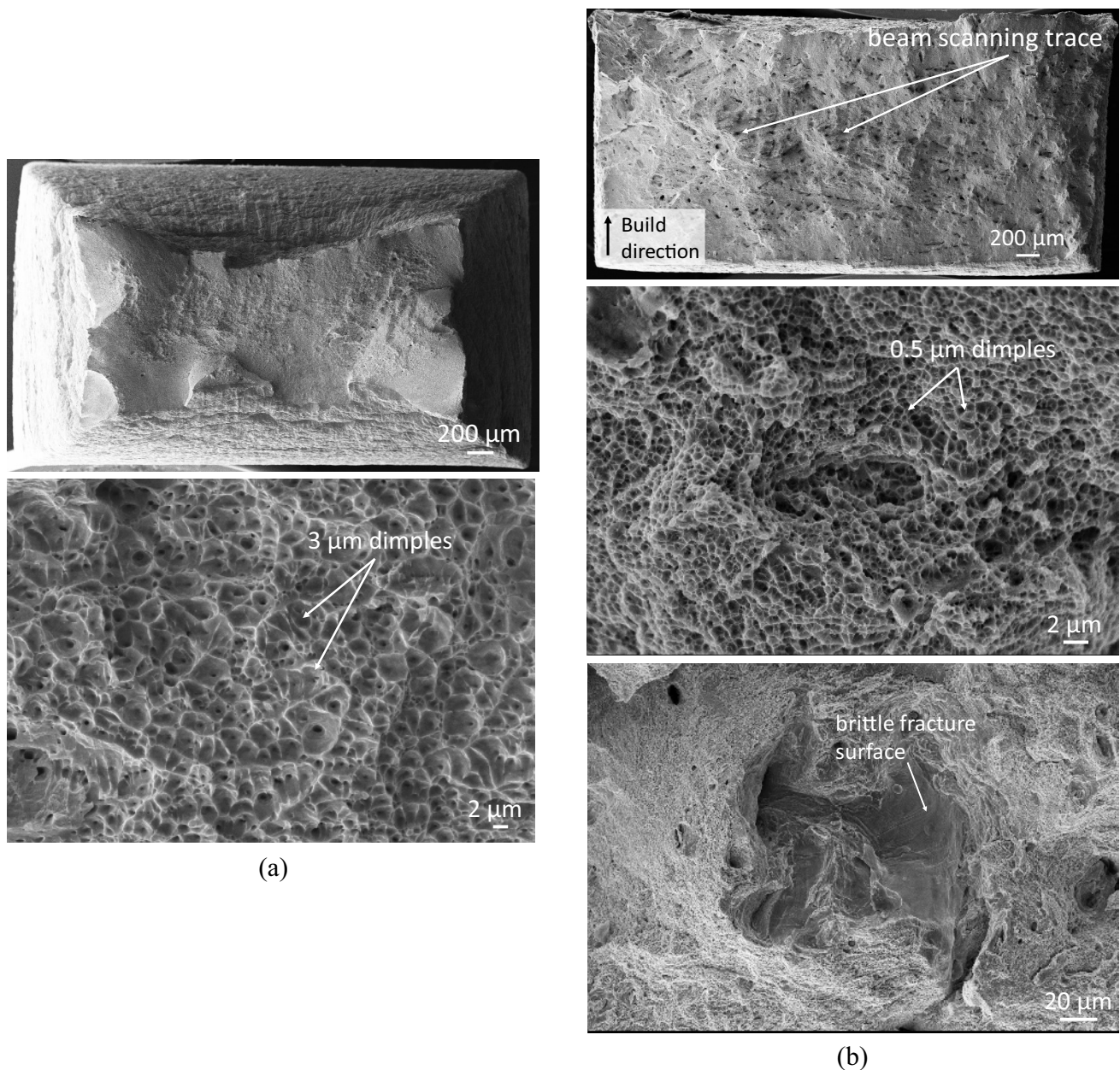


Fig. 11 Fracture surface observation for quarto plate AISI 316L (a) and LPBF horizontal (b) after tensile tests

LPBF products, or if modifications or new specific rules are needed.

3.2.1 Porosity of the welded samples

After polishing the welded samples, the quarto plate parts showed high density and a few imperfections, giving a 99.98% density (Fig. 12), and a maximum dimension for the pores of 80 μm. After welding, the LPBF parts of the welded samples still showed a large number of pores having average diameter 30 μm. The horizontal specimen showed a 99.52% density, the inclined specimen 99.70%, and the

vertical specimen 99.85%. The porosity decreased in terms of pore density and dimensions close to the weld seam, however, being the pore distribution not uniform along the samples, the density variation could not be reliably quantified to study the density sensitivity to welding thermal cycles.

3.2.2 Microhardness of the welded samples

The microhardness measures on horizontal, inclined and vertical welded samples are shown in Fig. 13. They are divided according to the distance from the top of the weld seam (from 1 to 9 mm far), and the three graphs in each plot

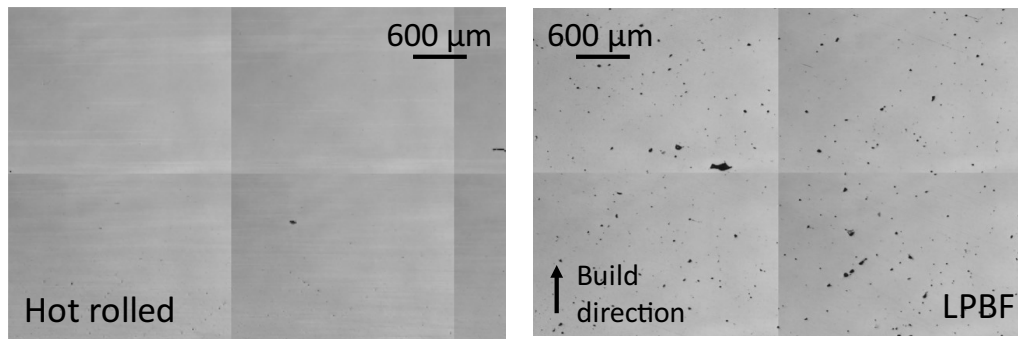


Fig. 12 Porosity of the quarto plate and LPBF parts of the horizontal welded sample

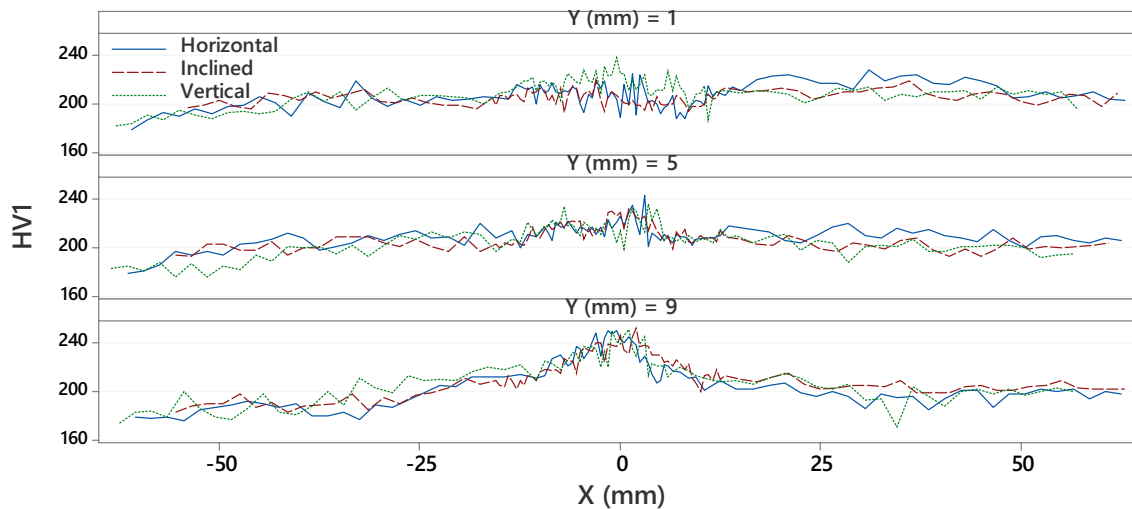


Fig. 13 Microhardness (HV1) values along the horizontal, inclined, vertical welded samples at three levels of sample thickness (1 mm, 5 mm and 9 mm from the weld seam top)

represent the measurements in the three sample types (i.e. horizontal, inclined, vertical). The microhardness analysis highlighted the variation induced by the welding thermal cycles close to the weld seam. The three samples demonstrated an instable evolution close to the weld seams, identifying the heat-affected zones. At 15 mm from the weld, the LPBF parts reached a stable microhardness trend, matching the base metal values (Fig. 8). Conversely, the quarto plate part showed a gentle constant decrease, and the microhardness values did not reach the nominal values in the whole sample length. The microhardness evolution across the thickness had a clear development in each sample, as the root of the weld showed a high microhardness value, while in the upper layers progressively decreased. This phenomenon is associated to the welding layers which superimposed one another, and gradually produced different thermal treatments. The microhardness analysis suggested that the LPBF steel is less sensitive to thermal treatments than quarto plate steel, and that the heat-affected zone can be identified as

a 15 mm offset of the weld seam edges on both the LPBF and quarto plate sides. The dimension of the HAZ will be compared to the microstructure analysis results in the next section, and possible mechanical weakening of this region will be evaluated during the tensile tests with DIC.

3.2.3 Microstructure of the welded samples

The microstructure observation of the welded samples showed the typical grain distribution of the AISI 316L quarto plate, and demonstrated that the welding thermal cycles did not affect the grain dimensions, having maintained the average dimensions of $30\ \mu\text{m}$. Austenite with delta ferrite was detected in weld seam, as well as both columnar dendrite and cellular structure (Fig. 14b). The fusion line of the welded region was clearly identified (Fig. 14a), and the weld seam observation after etching highlighted the welding layers shape having a medium width of 3 mm, 30 times larger than the medium dimension of the melt pools from

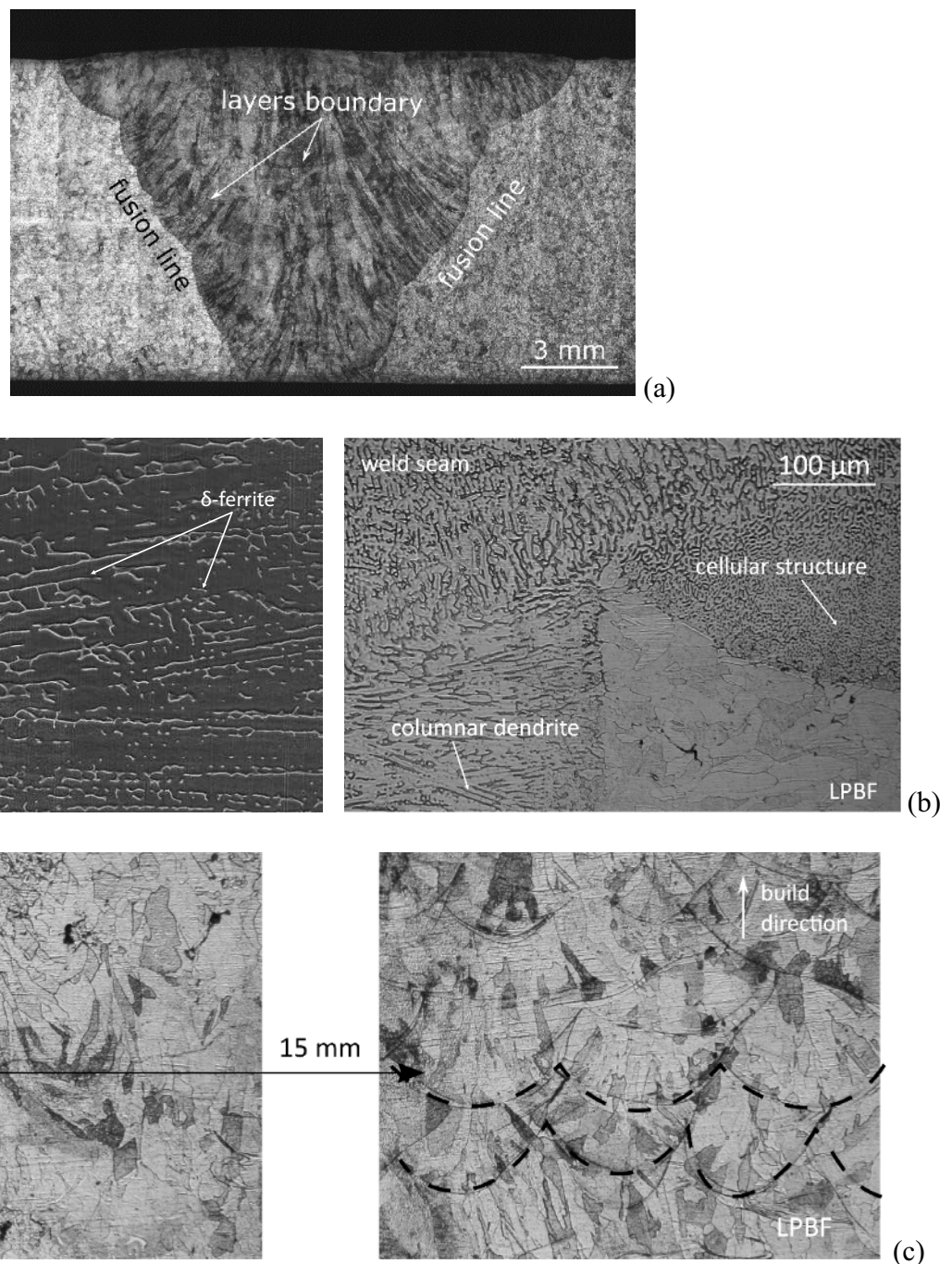


Fig. 14 Weld region of the horizontal welded sample (a); microstructure of the weld seam, and of its interface between with the LPBF part (b); differences in microstructure from the HAZ and the LPBF not affected by the welding thermal cycles (c)

the LPBF process. In the LPBF part, the chemical etching showed the typical LPBF elongated grains and the melt pools, having medium width 100 μm , and depth 40 μm . The differences among the weld seam, quarto plate and LPBF parts suggested that the weld seams could have its own properties, and it should be considered as a third part in the hybrid welded samples. Closes to the weld seam, up to

15 mm from the interface with the LPBF part, the melt pools were no more visible in all the samples. This highlighted the region mostly affected by the thermal cycle (Fig. 14c), and confirmed the HAZ dimension quantified during the micro-hardness analyses. Despite the effect of the welding process on the melt pools, the dimensions and orientation of the grains did not showed any relevant change along the samples

length, confirming the observations from the microhardness analyses about the limited effect of arc welding on the LPBF material.

3.3 Static tensile behaviour of the welded LPBF-quarto plate samples

During the tests, the samples showed a ductile behaviour with, first, a deterioration of the weld, and then an initial

deformation of the quarto plate part. These phenomena are followed by a strain concentration in the LPBF part, its necking and rupture (Fig. 18b). This observations fitted the strain concentrations evolutions identified by the DIC (Fig. 15a), which highlighted the hybrid behaviour of the welded samples (Fig. 15b), and to prove the DIC reliability as agreeing with the results from the traditional tensile tests. The hybrid samples (Fig. 15b) demonstrated a

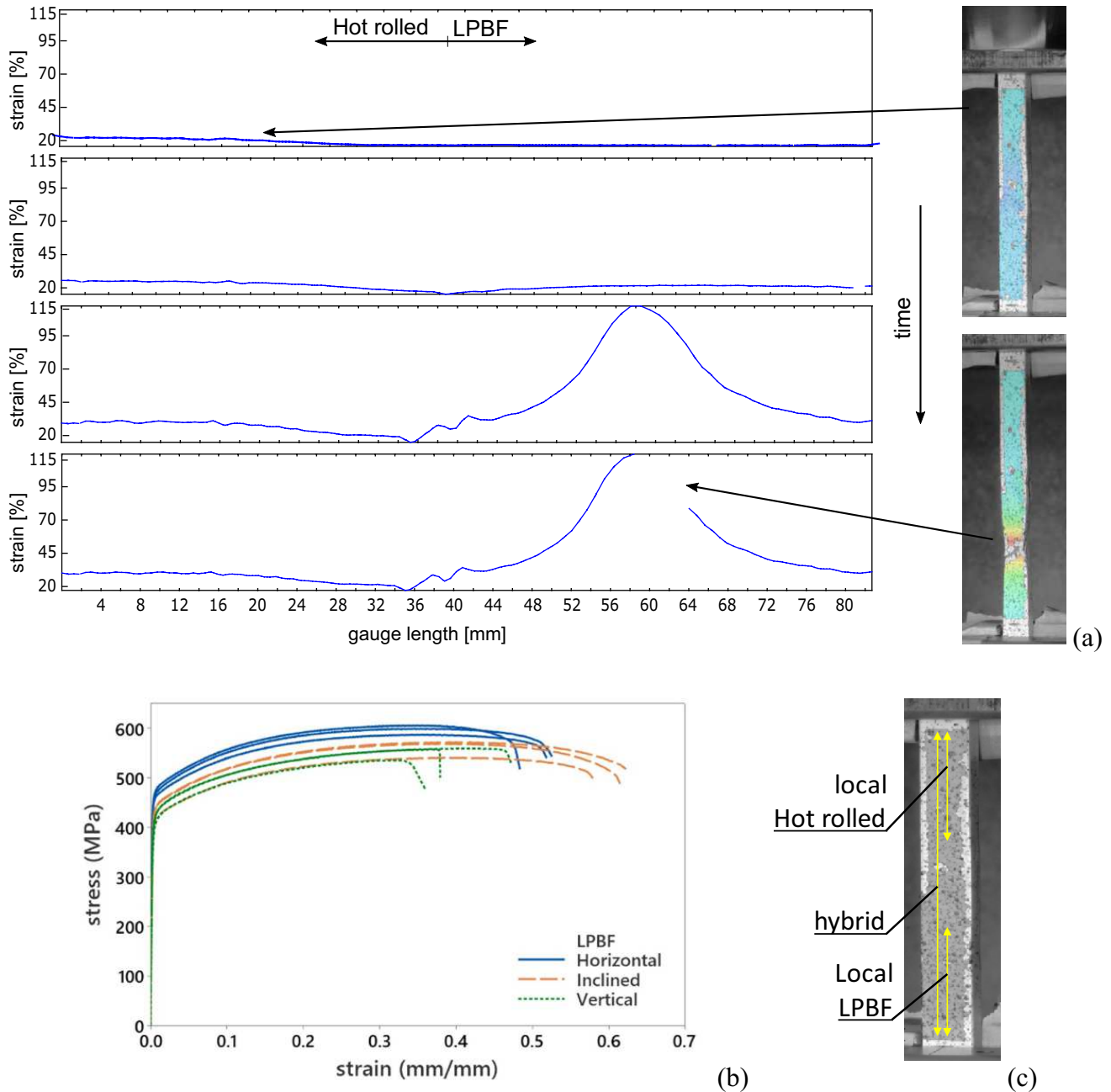


Fig. 15 Strain distribution in the most relevant steps of the tensile test with DIC (a); stress–strain curve of the welded samples (b); location of the virtual extensometers (c)

non-linear elasto-plastic behaviour with gradual yielding, and did not show a strong anisotropy.

The application of virtual local extensometers (Fig. 15c) to the weld seam, the quarto plate and LPBF parts captured their stress–strain responses (Figs. 16, 17), and particularly identified the anisotropic behaviour of the LPBF parts (Fig. 18a). A relevant gap is clear between the horizontal welded samples and the others (Fig. 17c), and the inclined samples showed low homogeneity in the curves (Fig. 16b) with respect to the horizontal and vertical samples (Fig. 16a, c). The weld seam showed a non-homogeneous distribution of properties due to the variability within the microstructure of the manually welded seam (Fig. 17a). Observing the local properties of the three parts of the hybrid samples (Fig. 16), it can be noticed a strong difference in yield strength between the quarto plate parts and the weld seam and LPBF ones. This observation is coherent with the microhardness measurements, since the weld seam and the LPBF parts had similar HV1, while the quarto plate part showed lower values (Fig. 13). Indeed, the Vickers hardness has been demonstrated to be directly proportional to the yield strength [50]. At the end, comparing the hybrid samples behaviour with the local properties of their parts, it is clear that the LPBF anisotropy is softened by the influence of the traditionally

manufactured components which demonstrated a homogeneous behaviour among all the sample types (Fig. 17b).

The properties of the LPBF and quarto plate steels before and after welding (Fig. 18a) revealed that the welding thermal cycles had a negligible effect on the yield and ultimate tensile strength values. Nevertheless, welding increased the elongation at ultimate tensile strength ϵ_u of the LPBF part by almost 10%, which could be considered during modelling and design of welded LPBF parts. These results mean that the base metal properties for both LPBF and quarto plate steels can be used to design welded samples, and just a reducing factor $\gamma = 0.85$ should be used to consider the actual strain at failure of the LPBF part. On the other hand, the elongation at failure ϵ_f showed higher values than the base metals, demonstrating an increase in ductility due to the welding thermal cycles. The last observation concerns the HAZ. There is not a distinguishable weakening in the regions close to the weld seam, and this confirmed the gradual microhardness variation from the weld seam to the base metals (Fig. 13), and the slight modification detected in the microstructure (Fig. 14c). These results demonstrated the good weldability of thick LPBF AISI 316L plates and quarto plate parts using arc welding, and provided the needed data

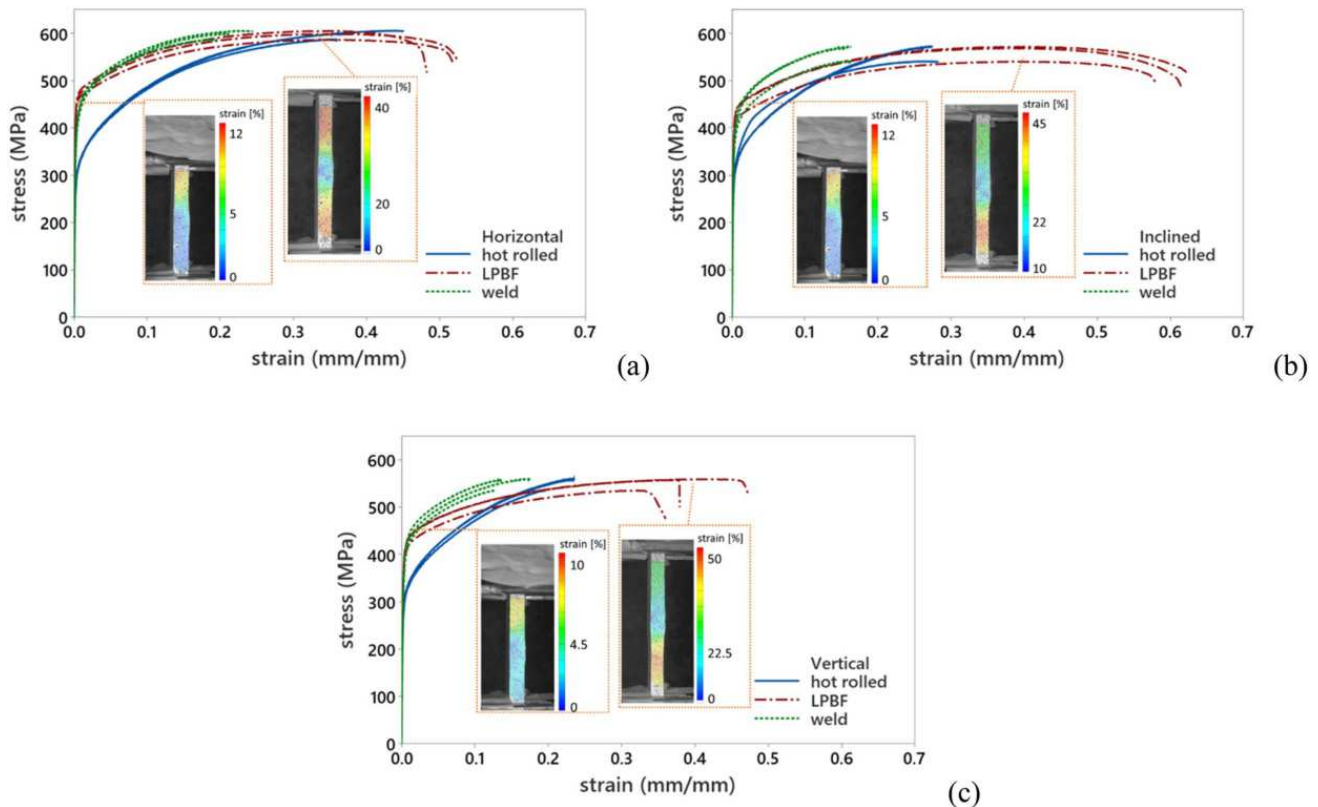


Fig. 16 Stress–strain curves of the three regions of the welded samples: quarto plate and LPBF parts, weld seam. The results are arranged according to the sample types: welded horizontal (a), welded inclined (b), welded vertical (c)

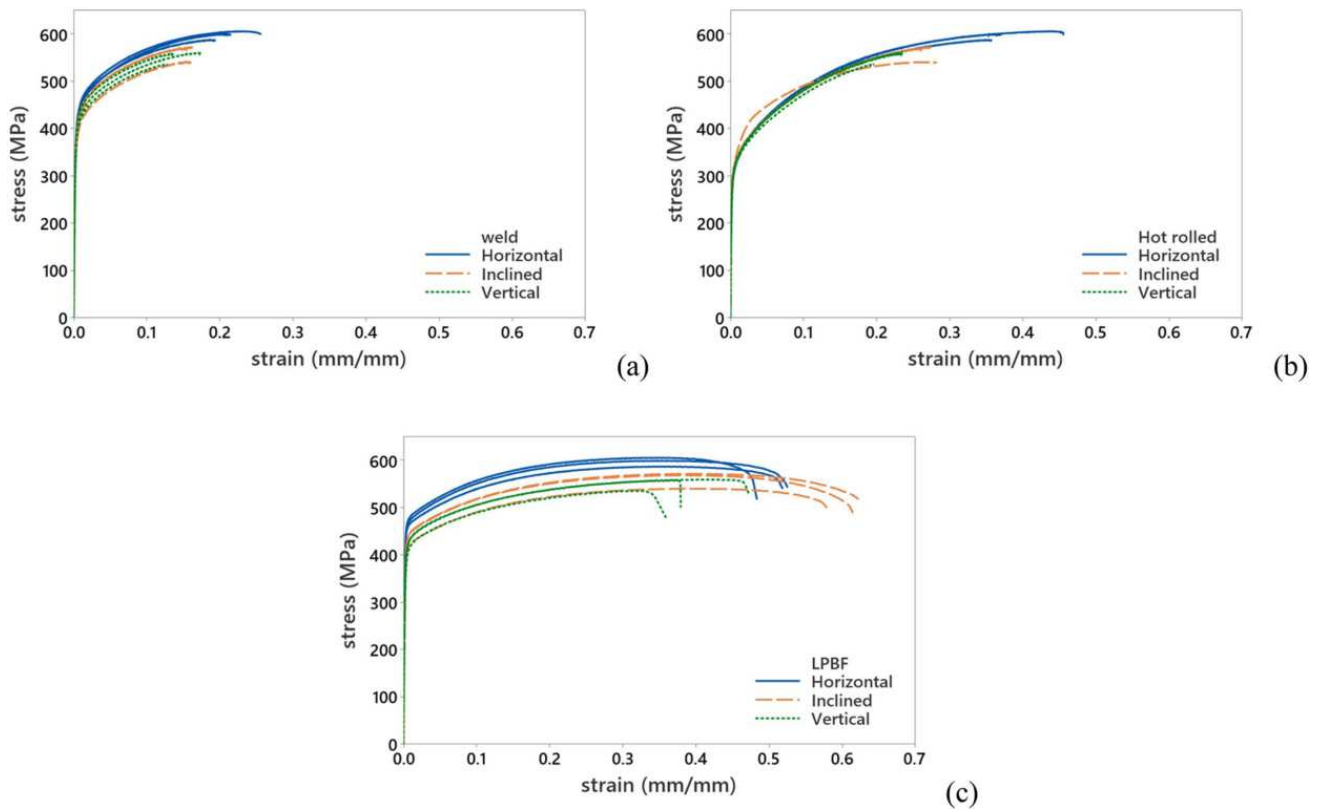


Fig. 17 Comparison among the local stress–strain curves of the welded samples: weld seams (a), quarto plate parts (b), LPBF parts (c)

to study the structural integrity of LPBF structural node to be welded to traditional profiles.

The LPBF process peculiarities were identified also in the fracture surface analysis. Several beam scanning traces (Fig. 19a) of the LPBF process emerged, highlighting that the melt pools boundaries were weak surfaces of the LPBF part. Unfused powder particles were detected (Fig. 19d), the formation of cracks followed these regions. The surfaces were mainly characterised by ductile dimples (Fig. 19c), but also brittle fracture regions arose (Fig. 19b). While further study of the process parameters may be carried out, such defects are inherent of the LPBF process and the layered material obtained through it.

4 Discussion

The present work aimed to design structural nodes produced with LPBF with properties and aesthetics as similar as possible to traditionally manufactured steel beams. This allows to homogenise the aesthetic and the performance of the differently manufactured components, in order to reduce the discontinuities. This discussion relates the experimental results to the most critical steps for the design of structural nodes, and identifies if the material properties are in

compliance with the standards or if these need to be adapted to the design of MAM-produced structural components.

Specifically, the study investigated and quantified the effect induced by arc welding on thick AISI 316L plates produced with additive manufacturing and traditional techniques (respectively, laser powder bed fusion and hot rolling). LPBF was considered in this research to produce steel nodes having complex shapes, with the aim of meeting the recent requests of the construction industry to simplify the assembling process of steel structures, reduce the discontinuities in welded structural joints, and the consumption of feedstock materials [9]. Considering the manufacturing of structural hybrid joints for industrially realistic applications, MAM revealed to be a viable technology to obtain benefits on the structural side and on the assembling and resource use ones [8, 14]. Despite the evaluated benefits, LPBF is not included in the Eurocode 3 [18] as manufacturing process for structural steel. Thus, a comprehensive evaluation of the material properties and accurate structural design are essential, and the fulfilment of the qualification and certification (CE marking [51]) are still needed to employ LPBF parts in the construction sector. The available studies from the literature were a good starting point for this study, but they do not provide enough information about thick plates and their

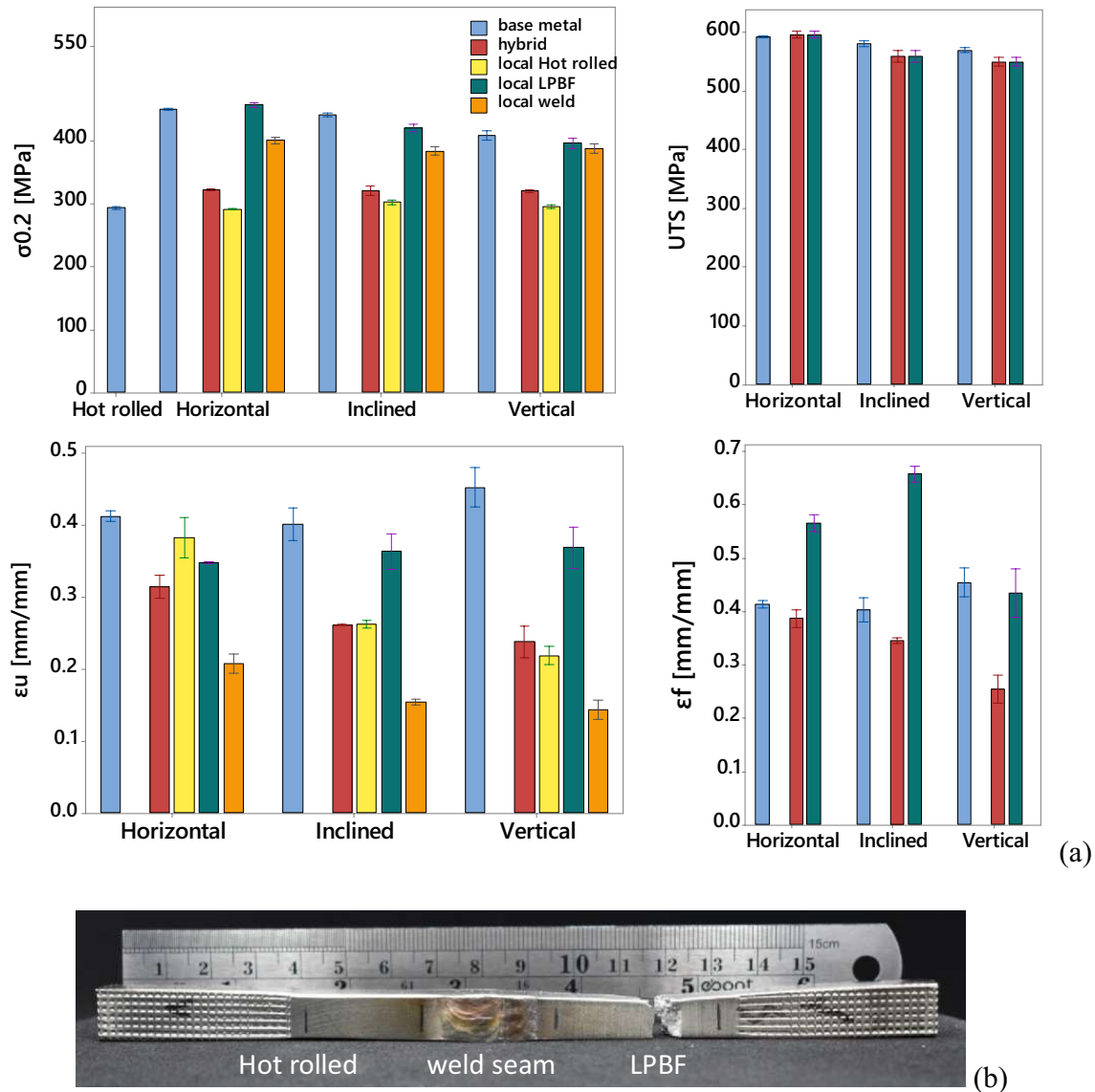


Fig. 18 Mechanical properties of the welded samples (hybrid) compared to base metals and local values from the three regions of the welded samples: LPBF, weld, quarto plate (a). $\sigma_{0.2}$ is the 0.2% proof

stress, UTS is the ultimate tensile strength, ϵ_u is the elongation at the ultimate tensile strength, ϵ_f elongation at failure. Macro image of the vertical welded sample after tensile test (b)

weldability to design structural complex components for future standardisation efforts. In particular, for constituent products not covered by design standards, ISO 1090-1 [16] and 1090-2 [17] demand to specify their properties. To such products, requirements from the relevant European products standards should be applied.

For the case study considered in this work, a 1D surface finishing is requested to employ LPBF products with traditionally manufactured profiles [52]. The 1D surface finishing represents a free of scale surface, ensuring good corrosion resistance (EN 10088-2 [45]), and corresponding to an Ra range typically between 3.5 and 7.5 μm . The results depict that the Ra values of LPBF as-built components, vary

between 10 and 20 μm . As a conservative approximation for the material allowance 4 times the value of Ra or the Rz value measurements can be considered for the successive surface finishing [53]. This means that the gross section of the as-built component should be enlarged by 80–160 μm to larger thickness. The dimensional adjustments to the designed geometry can be applied according to the surface finish requirement as well as inclination with respect to the build platform.

The process parameters are a crucial aspect for additive manufacturing, as they determine the quality of the products and the lead time for the production. Often the process parameters are set through the analysis of porosity followed

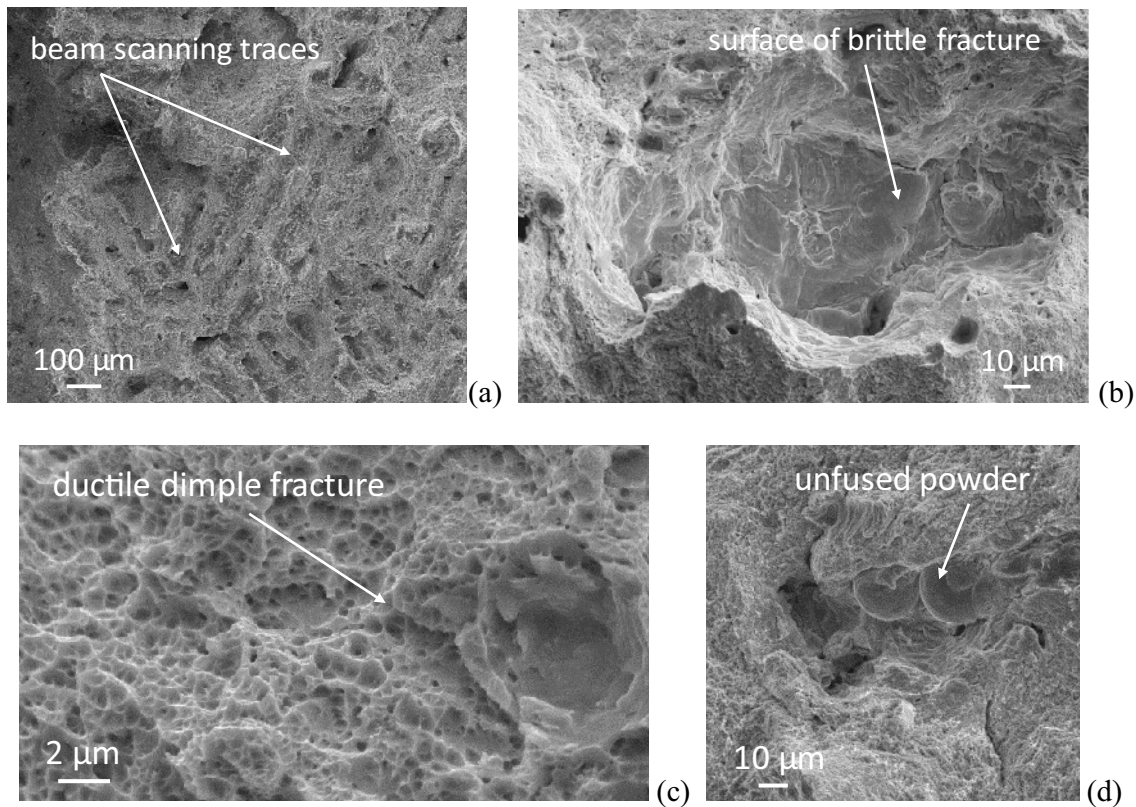


Fig. 19 Images of the vertical welded sample after the test and fracture surface details: scanning traces (a), brittle fracture surface (b); small ductile dimples (c); unfused powder (d)

by static tensile testing. Producing thick samples with high productivity rates provided products adequately fused without excessive porosity and adequate tensile strength. The fracture analysis on the LPBF and hybrid samples on the other hand showed the presence of local defects and the traces of the layered material structure. Further improvement of LPBF process stability may be carried out to go towards properties in compliance with the Eurocodes: dedicated post-processing treatments and inline process control. Hot isostatic pressing (HIP) may allow for a better bonding between the layers and help close some of the pores. Inline process monitoring can help with the process instabilities such as defected recoating, heat build-up, and spatter related issues, which may all cause local porosities [46, 47]. Such solutions are still to be developed for a wider industrial use.

Since additive manufacturing is not yet included as an allowed process for structural steel, a comparison to the requirements for traditional steels is the pathway to the certification of the process and the products. For traditional structures international standards provide rules and analyses to ensure a correct and safe design [18]. The first analysis that structural design requires is about the entire structure. Complex structures which need also optimisation processes are generally studied using global plastic analyses, since they

are more reliable than elastic analyses for the considered cases. The materials involved in the structures shall respect ductility conditions to ensure a safe development of the components' plasticity. In this regard, Eurocode 3 [18, 54] states that the plastic analyses are admissible if the ratio between the ultimate tensile strength and the yield strength of the material satisfy the expression $\frac{f_u}{f_y} \geq 1.10$, and the elongation at failure is never less than 15%. Our results revealed that the lowest $\frac{f_u}{f_y}$ ratio is equal to 1.31 in an horizontal sample, while the lowest elongations at fracture rose in an inclined sample with the value 33.4%, and in the LPBF part in the least ductile welded sample (welded vertical) reaching the 43.4%. These values prove the capacity of the material to develop sufficient plasticity to allow plastic analyses.

Going into the detail of node design, the components need to be verified in order to respect the performances required by the structure. The complex LPBF-produced node has both an unconventional shape and a non-standard production process. This denies the use of the rules for traditional components, and requires specific numerical analyses with properly defined numerical models. Indeed, AISI 316L quarto plate can be modelled as suggested by Eurocode 3 [54, 55], but these rules are not reliable for non-certified

production processes for structural steel. A relevant peculiarity of LPBF products in contrast with standard steel is its anisotropy. It is well known that quarto plate parts have their own anisotropy, which is evaluated through the plastic strain ratio [56]. Such anisotropy is negligibly small during the design phase [45]. The LPBF-produced components investigated in this study showed a slight anisotropy (Fig. 10). While quarto plate profiles are generally employed along their direction of highest resistance, the production as a single component of the LPBF node could require the involvement of the directions of the lowest resistance of the material. In particular, LPBF steel demonstrated anisotropy in both the elastic and plastic phase. The mechanical properties gathered in this study allow to model a transversely isotropic elastic phase and anisotropic yielding through Hill's criterion [57]. With this material model, a comparative analysis on the optimised node can be performed through numerical simulations by implementing both isotropic and anisotropic material models. The results would quantify the effect (in terms of stress and strain concentrations) that the anisotropy has on the node behaviour when combined with complex geometries. If the materials have a weak anisotropy, it could happen that the state of stress and strain obtained by modelling the material as anisotropic are similar to the results from isotropic models. In this regard, it would be interesting to identify a threshold value for the anisotropy magnitude (e.g. Zener ratio, Δr -value) for which the design with a isotropic material model is acceptable. Then, once defined a proper model, the node's integrity and performances can be verified by applying the loading conditions from the structural analysis, and computing the stresses and strain inside the node. The simulations results would prove if the node satisfy the requirements imposed by the structural scheme (hinge, rigid or semi-rigid joints) from a bearing and rotational capacities points of view.

The integrity of the weld has to be evaluated along with the node itself. The weldability of stainless steels is discussed in EN 1011-3 [40], and GTAW is assigned as suitable for welding AISI 316L. GTAW significantly reduced the elongation at ultimate tensile strength of the LPBF part by 10%, while the HAZ did not show relevant weakening. The reduced elongation at the ultimate tensile strength should be taken into account by considering a correcting parameter $\gamma = 0.85$ for the LPBF steel. For a conservative design and to limit the computational costs, this reducing parameter could be considered for modelling the material of the whole node. Indeed, the length of the node region showing the ultimate elongation reduction has not been measured, and the definition of a specific model for the heat-affected region would be nor possible neither much relevant for the integrity assessment of the joint. Another parameter to take into account is the increased elongation at failure after welding. The base metal properties could be considered to perform

the design on the safe side, since the vertical orientation did not show significant increase of the strain at failure. Concerning the weld seam verification, the conventional rules would be adopted as it was performed according to standard procedures, and it demonstrated a strong bond with the base metals. The directional method [20] is the most reliable approach to verify the welding as it computes the internal forces of the weld seam, and it is the less approximated on the experience. Numerical analyses on the welded joints can provide the actions which develop in the weld seam, and the comparison with the analytical ones can demonstrate the reliability of the verification from Eurocode 3 [20].

Besides the mechanical performances, the potentialities of implementing MAM nodes in traditional steel structures touch several aspects. LPBF can provide benefit in terms of labour content and resources use, and the optimised geometry can have inner space for positioning structural monitoring devices for durability assessment of the components. In case of node substitution during the structure life, the designers can improve the node performance and durability according to the information from structural monitoring, and with low design and customisation costs. The last example of advantage concerns the assembling procedure. Each node geometry could be characterised with a unique shape detail, which can be assigned by programming CAD software, and which can be used as identification parameter for the correct placement of the node. This procedure could help in assembling those structures composed of large amount of nodes having different shapes. MAM has multiple potentialities, and once the research would have defined design process and verifications, designer could fully exploit them.

5 Conclusions

Resource efficiency and geometrical advantages of laser powder bed fusion (LPBF) show great promise for the construction sector. However, the lack of experience and adequate design rules slows the industrial pick-up of metal additive manufacturing (MAM) processes. This work proposed a framework towards the design, production and verification of hybrid LPBF-quarto plate structural stainless steel nodes joined by welding. The study was guided by the analysis of a case of structural nodes and the main requirements for structural steel and joints design for manufacturing processes certified for the structural applications.

It is difficult to design and verify steel products manufactured through processes not classified by the international standards for constructions. Indeed, most of the rules are addressed to the traditional production processes, and just a few recommendations do not refer to specific techniques. However, all these general requirements for the use of steels in civil structures were satisfied by the

LPBF-produced 10-mm-thick AISI 316L plates. To go further in the analysis, the LPBF-produced AISI 316L was also compared to the certified products for civil structures, resulting in matching all the required mechanical properties. Despite this agreement with the main international codes, the stochastic nature of the porosity found in the LPBF products render their failure difficult to be predicted via conventional analysis methods. This needs further investigation to identify its influence on complex shapes behaviour, and to define threshold values to consider the material isotropic as already done for rolled steels. Concerning the design of the hybrid joints produced by welding LPBF and quarto plate steel parts, the mechanical properties of the base metals can be used for the design, and just a reducing factor for the strain at ultimate tensile strength can be taken into account. Concerning the welded hybrid node, the designer can adopt the directional method which considers the internal stresses in the weld seam for the numerical analyses. Indeed, this study provided the needed data to build reliable numerical models to assess the integrity of the nodes for its specific applications. Due to a lack of international standards, this is the most suitable route to verify the node design and to optimise it. The fatigue performance of the hybrid components will also be assessed in the future works. Along with the overall fatigue performance, the main defect type leading to the failure will be important to evaluate. In a complex system of LPBF-produced part together with a welded region, it is important to assess whether the LPBF related defects or the heat-affected zone due to the welding process will generate the crack initiation and propagation zones.

The next steps of this work will develop these numerical models to perform structural integrity analyses, and to investigate the influence of the LPBF steel anisotropy on the node behaviour. Such approach is expected to be crucial for future certification of LPBF-produced structural products, and for standardisation efforts concerning node design and verification. Overcoming standardisation and certification issues will open a wider field of exploration to the designers so that they can better exploit the mechanical and environmental advantages, and integrate strategies to improve the assembling and the maintenance procedures.

Acknowledgements The authors acknowledge CIMOLAI S.p.A. for the technical support and expertise in the field, and for providing the case study details.

Author contributions MC: conceptualisation; methodology; formal analysis; writing—original draft. AGD: conceptualisation; methodology; writing—original draft. AK: conceptualisation; writing—original draft. FB: supervision; writing—review and editing. CAC: supervision; writing—review and editing. BP: supervision; writing—review and editing.

Funding Open access funding provided by Politecnico di Milano within the CRUI-CARE Agreement. This work has been realised as preliminary study for the research project CONSTRUCTADD EU-RFCS 101057957 (<http://www.constructadd.eu>), funded by the European Union. Views and opinions expressed are, however, those of the authors only and do not necessarily reflect those of the European Union or Research Fund for Coal and Steel. Neither the European Union nor the Research Fund for Coal and Steel can be held responsible for them.

Data availability Data will be made available on request.

Declarations

Conflict of interest The authors declare that they have no known competing financial interests or personal relationships that could have appeared to influence the work reported in this paper.

Open Access This article is licensed under a Creative Commons Attribution 4.0 International License, which permits use, sharing, adaptation, distribution and reproduction in any medium or format, as long as you give appropriate credit to the original author(s) and the source, provide a link to the Creative Commons licence, and indicate if changes were made. The images or other third party material in this article are included in the article's Creative Commons licence, unless indicated otherwise in a credit line to the material. If material is not included in the article's Creative Commons licence and your intended use is not permitted by statutory regulation or exceeds the permitted use, you will need to obtain permission directly from the copyright holder. To view a copy of this licence, visit <http://creativecommons.org/licenses/by/4.0/>.

References

- Bernuzzi C, Cordova B (2016) Structural steel design to Eurocode 3 and AISC specifications. Wiley, Hoboken
- DebRoy T et al (2019) Scientific, technological and economic issues in metal printing and their solutions. *Nat Mater* 18(10):1026–1032
- Debroy T et al (2018) Additive manufacturing of metallic components—process, structure and properties. *Prog Mater Sci* 92:112–224
- Herzog D, Seyda V, Wycisk E, Emmelmann C (2016) Additive manufacturing of metals. *Acta Mater* 117:371–392
- Delgado Camacho D et al (2018) Applications of additive manufacturing in the construction industry—a forward-looking review. *Autom Constr* 89:110–119
- Buchanan C, Gardner L (2019) Metal 3D printing in construction: a review of methods, research, applications, opportunities and challenges. *Eng Struct* 180:332–348
- Ribeiro TP, Bernardo LFA, Andrade JMA (2021) Topology optimisation in structural steel design for additive manufacturing. *Appl Sci* 11(5):2112
- Chierici M, Berto F, Kanyilmaz A (2021) Resource-efficient joint fabrication by welding metal 3D-printed parts to conventional steel: a structural integrity study. *Fatigue Fract Eng Mater Struct* 44:1271–1291
- Kanyilmaz A et al (2021) Role of metal 3D printing to increase quality and resource-efficiency in the construction sector. *Addit Manuf* 50:102541
- du Plessis A et al (2019) Beautiful and functional: a review of biomimetic design in additive manufacturing. *Addit Manuf* 27:408–427

11. Kaethner SC, Burrigge JA (2012) Embodied CO₂ of structural frames. *Struct Eng* 90(5):33–40
12. Peng T, Kellens K, Tang R, Chen C, Chen G (2018) Sustainability of additive manufacturing: an overview on its energy demand and environmental impact. *Addit Manuf* 21:694–704
13. Kanyilmaz A, Berto F, Paoletti I, Caringal RJ, Mora S (2020) Nature-inspired optimization of tubular joints for metal 3D printing. *Struct Multidiscip Optim* 63:767–787
14. Chierici M, Berto F, Kanyilmaz A, Castiglioni CA (2022) Life cycle inventory analysis for resource-efficient structural steel nodes: metal 3D printing or traditional manufacturing?, In: *Structures and Architecture A Viable Urban Perspective?*, 1st edition, CRC Press, ISBN: 9781003023555
15. Moynihan MC, Allwood JM (2014) Utilization of structural steel in buildings. *Proc R Soc A Math Phys Eng Sci* 470:20140170
16. European Committee for Standardization (2011) EN 1090-1 (2009) execution of steel structures and aluminium structures—part 1: requirements for conformity assessment of structural components
17. European Committee for Standardization (2018) EN 1090-2 (2019) execution of steel structures and aluminium structures—part 2: technical requirements for steel structures
18. European Committee for Standardization (2005) EN 1993-1-1 (2005) Eurocode 3: design of steel structures—part 1-1: general rules and rules for buildings, pp 1–91
19. European Committee for Standardization (2006) EN 1993-1-4 (2006): Eurocode 3: design of steel structures—part 1-4: general rules—supplementary rules for stainless steel, pp 1–35
20. European Committee for Standardization (2005) EN 1993-1-8 (2005)—Eurocode 3: design of steel structures—part 1-8: design of joints, pp 1–134
21. Buchanan C, Matilainen V-P, Salminen A, Gardner L (2017) Structural performance of additive manufactured metallic material and cross-sections. *J Constr Steel Res* 136:35–48
22. Yakout M, Elbestawi MA, Veldhuis SC (2019) Density and mechanical properties in selective laser melting of Invar 36 and stainless steel 316L. *J Mater Process Technol* 266:397–420
23. Casati R, Lemke J, Vedani M (2016) Microstructure and fracture behavior of 316L austenitic stainless steel produced by selective laser melting. *J Mater Sci Technol* 32(8):738–744
24. Tolosa I, Garcíandía F, Zubiri F, Zapirain F, Esnaola A (2010) Study of mechanical properties of AISI 316 stainless steel processed by ‘selective laser melting’, following different manufacturing strategies. *Int J Adv Manuf Technol* 51:639–647
25. Hitzler L, Hirsch J, Heine B, Merkel M, Hall W, Öchsner A (2017) On the anisotropic mechanical properties of selective laser-melted stainless steel. *Materials (Basel)* 10(10):1136
26. Shrestha R, Simsiriwong J, Shamsaei N (2019) Fatigue behavior of additive manufactured 316L stainless steel parts: effects of layer orientation and surface roughness. *Addit Manuf* 28:23–38
27. Charmi A et al (2021) Mechanical anisotropy of additively manufactured stainless steel 316L: an experimental and numerical study. *Mater Sci Eng A* 799:140154
28. Wang D, Mai S, Xiao D, Yang Y (2016) Surface quality of the curved overhanging structure manufactured from 316-L stainless steel by SLM. *Int J Adv Manuf Technol* 86(1–4):781–792
29. Zuback JS, DebRoy T (2018) The hardness of additively manufactured alloys. *Mater (Basel)* 11(11):2070
30. Laitinen V (2015) Weldability of powder bed fusion fabricated stainless steel 316L sheets to cold rolled sheet metal. Master’s thesis, pp 1–73
31. Zhang R et al (2021) Mechanical properties and microstructure of additively manufactured stainless steel with laser welded joints. *Mater Des* 208:109921
32. Mohyla P et al (2020) Analysis of welded joint properties on an AISI316L stainless steel tube manufactured by SLM technology. *Materials (Basel)* 13(19):4362
33. Previtali B, Demir AG, Bucconi M, Crosato A, Penasa M (2017) Comparative costs of additive manufacturing vs. machining: the case study of the production of forming dies for tube bending. *Solid Free Fabr Symp*, pp 2816–2834
34. Merklein M, Schulte R, Papke T (2021) An innovative process combination of additive manufacturing and sheet bulk metal forming for manufacturing a functional hybrid part. *J Mater Process Technol* 291(July 2020):117032
35. Pasang T et al (2019) Microstructure and mechanical properties of welded additively manufactured stainless steels SS316L. *Met Mater Int* 25(5):1278–1286
36. Research and Markets (2020) Global Additive Manufacturing Market and Technology Forecast to 2028, pages 1–274, ID: 5144559, <https://www.researchandmarkets.com/reports/5144559/global-additive-manufacturing-market-and#src-pos-1>
37. ASTM International (2016) ASTM F3184-16. Standard specification for additive manufacturing stainless steel alloy (UNS S31603) with powder bed fusion. pp 1–9, ICS Code: 25.030. <https://doi.org/10.1520/F3184-16>
38. Demir AG, Colombo P, Previtali B (2017) From pulsed to continuous wave emission in SLM with contemporary fiber laser sources: effect of temporal and spatial pulse overlap in part quality. *Int J Adv Manuf Technol* 91:2701–271
39. Demir AG, Previtali B (2017) Investigation of remelting and preheating in SLM of 18Ni300 maraging steel as corrective and preventive measures for porosity reduction. *Int J Adv Manuf Technol* 93:2697–2709
40. European Committee for Standardization (2000) BS EN 1011-3 (2000)—welding. Recommendations for welding of metallic materials. Arc welding of stainless steels
41. European Committee for Standardization (2016) EN ISO 17637 (2016) non-destructive testing of welds. Visual testing of fusion-welded joints
42. European Committee for Standardization (2019) EN ISO 3183 (2019) petroleum and natural gas industries. Steel pipe for pipeline transportation systems
43. European Committee for Standardization (2018) EN ISO 6507-1 (2018) standards publication metallic materials—Vickers hardness test
44. Morozov EV, Vasiliev VV (2003) Determination of the shear modulus of orthotropic materials from off-axis tension tests. *Compos Struct* 62:379–382
45. European Committee for Standardization (2014) EN 10088 (2014)—stainless steels—part 2: technical delivery conditions for sheet/plate and strip of corrosion resisting steels for general purposes, no. December 2014, pp 1–58
46. Repossini G, Laguzza V, Grasso M, Colosimo BM (2017) On the use of spatter signature for in-situ monitoring of Laser Powder Bed Fusion. *Addit Manuf* 16:35–48
47. Vasileška E, Demir AG, Colosimo BM, Previtali B (2022) A novel paradigm for feedback control in LPBF: layer-wise correction for overhang structures. *Adv Manuf* 10(2):326–344
48. Ronneberg T, Davies CM, Hooper PA (2020) Revealing relationships between porosity, microstructure and mechanical properties of laser powder bed fusion 316L stainless steel through heat treatment. *Mater Des* 189:108481
49. (2000) Mechanical testing and evaluation. In: *ASM handbook*, vol 8, pp 1–959
50. Tabor D (1951) *The hardness of metals*. Oxford University Press
51. Official Journal of the European Union (2011) Regulation (EU) No 305/2011 of the European Parliament and of the Council of 9th March 2011 laying down the harmonised conditions for

- the marketing of construction products and repealing Council Directive 89/106/EEC
52. European Committee for Standardization (2006) BS EN 10021 (2006) General technical delivery conditions for steel products
 53. Scarpellini A, Schito P, Demir AG (2023) Feasibility of using bio-mimicking fish scale textures in LPBF for water drag-reducing surfaces. *Prog Addit Manuf.* <https://doi.org/10.1007/s40964-023-00394-y>
 54. International Organization for Standardization (2006) EN 1993-1-4 (2006): Eurocode 3: design of steel structures—part 1–4: general rules—supplementary rules for stainless steel, pp 1–35
 55. European Committee for Standardization (2006) EN 1993-1-5 (2006) Eurocode 3—design of steel structures—part 1–5: plated structural elements
 56. European Committee for Standardization (2020) BS EN ISO 10113 (2015) metallic materials—sheet and strip—determination of plastic strain ratio
 57. Hill R (1948) A theory of the yielding and plastic flow of anisotropic metals. *Proc R Soc Lond* 193:281–297

Publisher's Note Springer Nature remains neutral with regard to jurisdictional claims in published maps and institutional affiliations.